Goblet cells mechanically breach the epithelial barrier in gut homeostasis

Justine Creff[1], Yuan He[2], Sandra Bernat-Fabre[1#], Etienne Buscail[3#], Salomé Neuvendel[1#], Vishnu Krishnakumar[1], Thomas Mangeat[4], Shi-Lei Xue[2*], Denis Krndija[1*]

[1]Molecular, Cellular and Development Biology Unit (MCD) – Centre de Biologie Intégrative (CBI), University of Toulouse, CNRS, Toulouse, France

[2]School of Life Sciences, Westlake University, Hangzhou, Zhejiang, PR China

[3]Department of Digestive Surgery, Colorectal Surgery Unit, Toulouse University Hospital, Toulouse, France

[4]LITC Core Facility, Centre de Biologie Intégrative (CBI), University of Toulouse, CNRS, Toulouse, France

[#]These authors contributed equally to this work

[*]Corresponding authors: xueshilei@westlake.edu.cn; denis.krndija@univ-tlse3.fr

Abstract

The intestinal epithelium has to maintain a tight barrier to the harsh luminal environment. The absorptive enterocytes have a polygonal and columnar shape, while mucus-producing goblet cells have a round apical cell shape and a bulky body, raising the question of how epithelial integrity is maintained around these cells. Here, we show that goblet cells induce tight junction fractures between neighboring enterocytes under homeostatic conditions *in vivo*. Through theoretical modeling and experimental perturbations, we demonstrate that these fractures arise from a two-component mechanical process: goblet cells push and deform enterocytes, promoting junctional rupture as a function of tissue rheology controlled by myosin II. These findings reveal that the mechanical interplay between goblet cells and neighboring enterocytes is critical for intestinal epithelial barrier integrity.

Introduction

Epithelia are specialized tissue barriers, with a critical role in separating internal and external environment and thus maintaining normal tissue function and homeostasis (*1*). The intestinal epithelium functions as a protective barrier throughout adult life, shielding the organism from continuous environmental insults (*2*), including extrinsic mechanical stresses from luminal contents and muscle-driven peristalsis (*3*, *4*) as well as intrinsic mechanical stresses due to rapid epithelial turnover (*5*). Adhesive cell junctions – including tight junctions (TJs), adherens junctions (AJs) and desmosomes – enable epithelial barrier, mechanical integrity and collective cell migration (*5*–*7*). TJs are continuous belt-like structures that encircle and seal the paracellular space and regulate the barrier permeability (*8*). AJs, which lie just beneath the TJs, couple the cytoskeletons of neighboring cells by linking transmembrane E-cadherins belts to the cortical actomyosin network, which stabilizes E-cadherin complexes (*9*–*11*). As a consequence, AJs are under tension and transmit subcellular forces exerted by actomyosin networks to the cortex (*12*). Junctional complexes are mechanosensitive and mechanoadaptive, integrating subcellular and tissue-level forces, and modulating cell behavior – e.g., junctional reinforcement upon mechanical load to maintain barrier integrity and tissue cohesion (*10*, *11*, *13*, *14*). Finally, desmosomal plaques are located basolaterally beneath the AJs and are associated to intermediate filaments. They were recently shown to passively respond to extrinsic forces by strain-stiffening, contributing to the mechanical resilience of epithelial tissues (*15*, *16*).

The intestinal epithelium consists of six different cell types, each with specialized functions and morphologies. Enterocytes, the main cell type, are absorptive cells with a columnar shape and a polygonal apical surface. The mucus-producing goblet cells (GCs), interspersed among enterocytes, are the second most abundant cell type and are characterized by their bulky, round-shaped bodies, due to the presence of large secretory granules (*17*–*19*). While numerous studies have focused on the secretory function of GCs, the impact of their unique geometry and mechanical properties on their integration into the epithelial tissue and the intestinal barrier remains entirely unknown.

Here, we report that under homeostatic conditions *in vivo*, GCs are physically associated with junctional fractures that occur between neighboring enterocytes in the small intestine. Using a combination of 3D tissue imaging, *in vivo* (mouse models), *ex vivo* (explants), and *in vitro* (organoids) force perturbations and theoretical modeling, we found that fracturing arises from the intrinsic mechanical properties and interplay between GCs and adjacent enterocytes. On the one hand, GCs compress and deform adjacent enterocytes, straining their intercellular junctions and promoting fracturing; on the other hand, fracturing depends on global tissue mechanics (rheology), which is controlled by myosin II activity.

Results

Goblet cells are associated with TJ fractures between adjacent enterocytes under homeostatic conditions

To investigate how GCs are integrated in the small intestinal epithelium, we first assessed TJs by immunofluorescence (ZO-1, occludin) on thick sections of adult murine intestine (jejunum), enabling high-resolution 3D imaging of the villus apical surface *en face* (Fig. 1A, S1A). GCs are easily identified due to their round apical shape and absence of an F-actin-rich brush border, in contrast to polygonal enterocytes, which was validated by staining for mucus (Fig. S1B). We observed that GCs are frequently (>50%) and significantly associated with fractures (Fig. 1A, S1A, arrows) in adjacent (1st neighbor) enterocyte-enterocyte (E-E) TJs. In contrast, we rarely observed (0.7%) fractures in E-E TJs non-adjacent to GCs (2nd neighbors or farther) (Fig. 1A, B, E). The fractures are wider proximal to the GCs, at the goblet-enterocyte-enterocyte (G-E-E) tricellular junctions, and become gradually narrower away from the GC along the E-E bicellular TJs (Fig. S1C). Importantly, we also observed fractures in healthy regions of human small intestinal biopsies (ileum) with the same frequency (Fig. 1C, D; Fig. S1D), suggesting that this phenomenon is conserved.

In addition, we assessed the presence of fractures at other junctional complexes - at AJ level, fractures were ≈3 times less frequent (18%) while no fractures were detected at desmosome level (Fig. S1E). We asked whether these fractures could be the result of extrinsic forces (e.g., luminal shear stress due to digesta flow) or interaction with gut microbiota or immune cells. Remarkably, we found GC-associated fractures in the murine embryonic villi (E16.5 embryos, early upon villi emergence), where digesta, immune system and microbiota are not yet present (Fig. S1F). To further assess whether GAFs are influenced by extrinsic cues, we turned to the murine small intestine 2D organoid model, which contains functional GCs and mucus, and whose accessible apical surface enables high-resolution imaging of the TJs (Fig. S2A, B) (*20*). Similar to the *in vivo* condition, 50% of GCs in the villus-like regions of 2D organoids were associated with TJ fractures (Fig. S2C-D). Together, these findings suggest that GC-associated fracturing is epithelium-autonomous, arising from intrinsic properties of the epithelial monolayer. We have termed this phenomenon "Goblet cell-Associated Fractures" (GAFs).

Interestingly, we observed an increase in GAF area (five-fold increase) when GCs were in close proximity, i.e., separated by only one row of neighboring cells, suggesting a cumulative effect (Fig. 1F-H). To determine whether GAFs represent a functional breach in the epithelial barrier, we evaluated the luminal accessibility of E-cadherin using a sequential staining approach in which the accessible extracellular domain of E-cadherin is labeled with specific antibodies prior to tissue permeabilization, followed by F-actin staining after permeabilization (Fig. S1G) (*21*). The accessible E-cadherin signal was detected only in GC-adjacent E-E junctions, with over 80% of GCs associated with accessible E-cadherin staining (Figure 1I, J), indicating that TJs around GCs

are indeed breached. Taken together, these data suggest that GCs locally disrupt junctional integrity in the gut epithelium under homeostatic conditions.

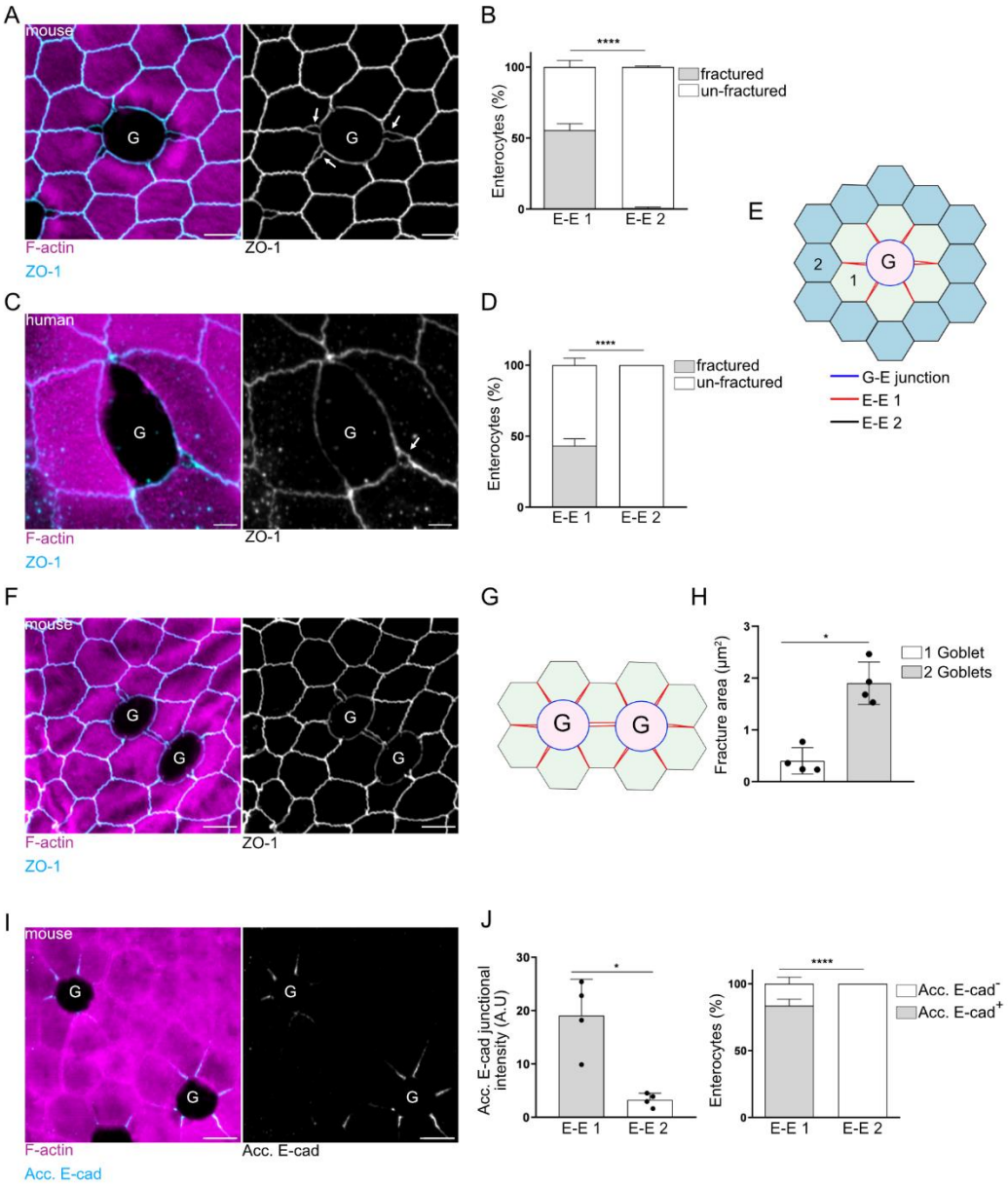

Figure 1: Goblet cells are associated with TJ fractures between adjacent enterocytes under homeostatic conditions. (A) Representative *en face* image of murine intestinal tissue. Maximum intensity projection (Z range, 2 µm). White arrows are showing fractures in enterocyte-enterocyte (E-E) 1st neighbor tight junctions (E-E 1). Scale bars, 5 µm. (B) Stacked bar graph showing average percentage of enterocytes associated with fractures (GAFs). Multiple t-test, ****: $p < 0.0001$; n=4 independent experiments. (C) Representative *en face* image of thick section of human intestinal ileum. Maximum intensity projection (Z range, 2.2 µm). White arrow is showing fractures in 1st neighbor E-E junctions. Scale bars, 5 µm. (D) Stacked bar graph showing average percentage of enterocytes associated with fractures (GAFs) in human tissue. Multiple t-test, ****: $p < 0.0001$; n=4 independent experiments.

Legend continued on next page

Figure 1 legend (continued)

(E) Schematic representation showing fractures are present in 1st neighbor E-E TJs (E-E 1, red) and absent in G-E (blue) and 2nd neighbor E-E TJs (E-E 2, black). (F) Representative image of two GCs in close proximity. Maximum intensity projection (Z range, 2.8 µm). ZO-1 (cyan); F-actin (magenta). Scale bars, 5µm. (G) Schematic representation showing the cumulative effect of 2 GCs on fracturing. (H) Bar chart displaying average fracture area between 2 GCs. Mann-Whitney test, *: $p < 0.05$; n=4 experiments. (I) Representative image of murine tissue stained for accessible E-cadherin (cyan) and F-actin (magenta). Maximum intensity projection (Z range, 3.18 µm). Scale bars, 5µm. (J) Left: Bar chart displaying average accessible E-cadherin junctional intensity; Mann-Whitney test, *: $p < 0.05$; n=4 experiments. Right: Stacked bar graph showing the average percentage of accessible E-cadherin-positive cells. Multiple t-test, ****: $p < 0.0001$. (n=3 experiments). Acc. E-cad, accessible E-cadherin.

Goblet cells mechanically compress the neighboring enterocytes, leading to their deformation and junctional fractures

Next, we investigated whether GC shape contributes to GAF formation. Unlike their slender enterocyte neighbors, GCs have a bulky body filled with mucus granules, which deforms the lateral walls of adjacent enterocytes (Fig. 2A). Furthermore, super-resolution imaging of desmoplakin, a marker of desmosomal outer dense plaques, revealed a significant and consistent two-fold decrease in intra-desmosomal space at the G-E junctions compared to E-E junctions (Fig. S3A), suggesting mechanical compression exerted by goblet cells.

From a physical perspective, the stereotypical outwards curvature of the G-E junction must arise from GCs having a larger pressure than enterocytes (see Theory Note for details), with the value of curvature reflecting a balance between the pressure difference and tension at the G-E boundary. This is also consistent with G-E junctions being smooth, whereas E-E TJs display substantial folds and wiggliness (Fig. S3B). Minimal physical modelling of GC geometry with a finite adhesion energy between enterocytes indeed predicts partial fracture above a critical pressure, as well as complete junctional fracture above another pressure threshold (Theory Note). Overall, this led us to the hypothesis that GCs exert pressure on their neighbors, straining E-E junctions while compressing G-E junctions, which could lead to junctional fracture.

To test this hypothesis directly and manipulate GC pressure, we treated mice with succinate, a microbial metabolite known to induce GC hypertrophy (increase in GC mucus volume) and hyperplasia (increase in GC number) (*22*). The succinate treatment led to a marked increase in GC mucus volume (control: 317.04 μm^3; succinate: 681.57 μm^3) (Fig. 2B, C); unexpectedly, GC numbers remained similar (Fig. S3D, E). Hypertrophic GCs were associated with significantly increased fracturing in adjacent E-E tight junctions, showing a three-fold increase in GAF area (control: 0.42 μm^2; succinate: 1.29 μm^2) and almost two-fold increase in GAF number (control: 53%; succinate: 95%) (Fig. 2D, E), while no decrease of ZO-1 junctional intensity was observed (Fig. S3F). These results were recapitulated in organoid monolayers, where GC hyperplasia and hypertrophy were induced by stimulating the GC fate by inhibiting the Notch and Wnt pathways (*23*) (Fig. S4).

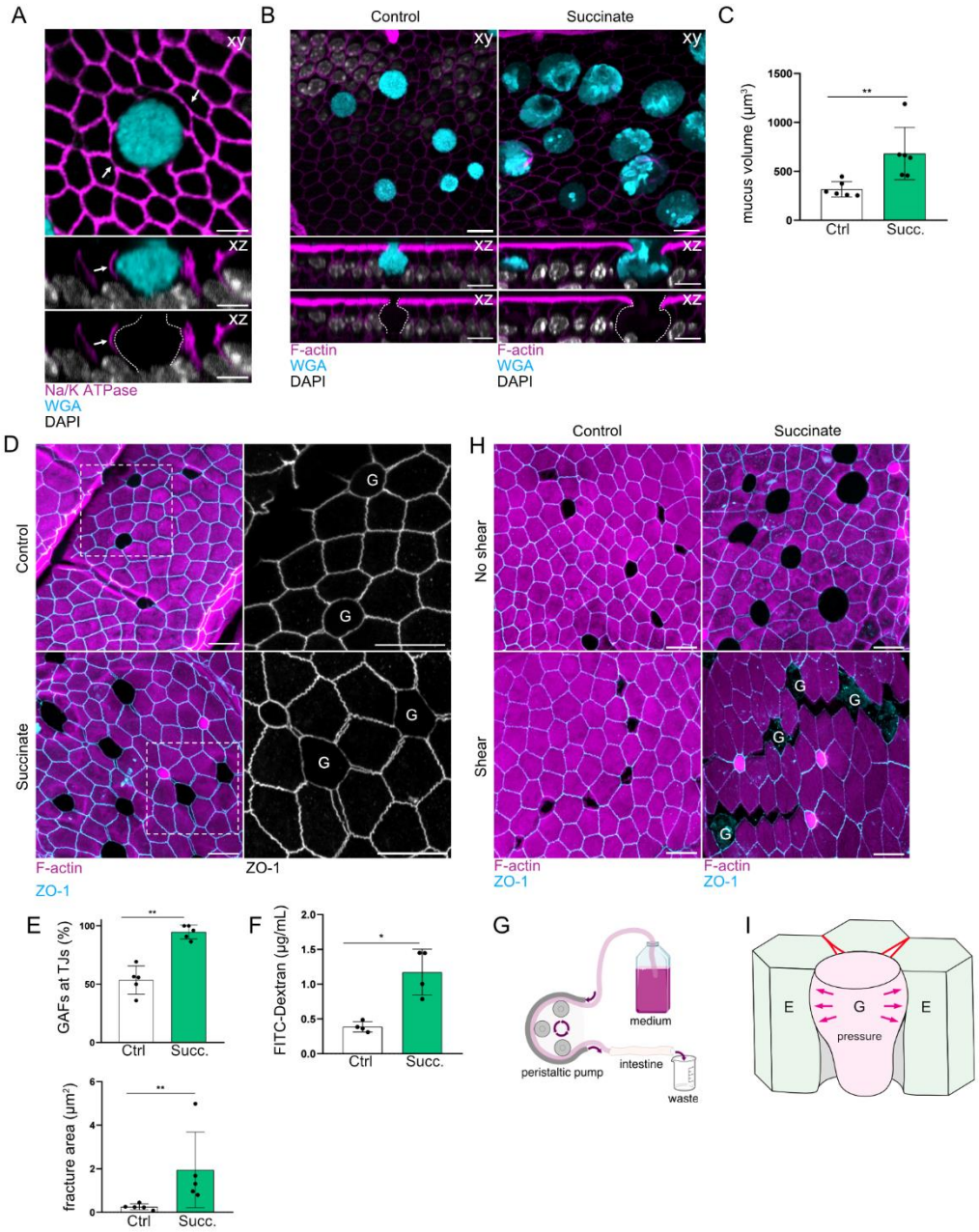

Figure 2: Goblet cells mechanically compress the neighboring enterocytes, leading to their deformation and junctional fractures. (A) Representative xy and xz confocal images from thick intestinal sections. White arrows are showing lateral deformation of GC-adjacent enterocytes. Scale bars, 5 µm. (B) Representative xy and xz images of control and succinate tissue showing increased mucus volume, and deformation of goblet-adjacent enterocytes. Scale bars, 10 µm. (C) Bar chart displaying average mucus volume. Mann-Whitney test. **: $p < 0.01$; n=6 experiments**.** (D) Representative images from control and succinate tissues. Boxed regions are shown in higher magnification. Maximum intensity projection (Z range, 4.8 µm, 2.7 µm). Scale bars, 10 µm. (E) Top: Bar charts displaying average percentage of GAFs at TJs level. Mann-Whitney test. **: $p < 0.01$. Bottom: Bar chart showing average fracture area. Mann-Whitney test. **: $p < 0.01$.; n=5 experiments. (F) Bar charts displaying average intestinal permeability. Mann-Whitney test. *: $p < 0.05$; n=4 experiments. (G) Schematic representation of experimental procedure to apply shear stress *ex vivo* on intestinal epithelium. (H) Representative images of control and succinate tissues submitted to luminal shear stress. Maximum intensity projection (Z range, 4.2 µm, 3.2 µm, 4.5 µm, 4.8µm). Scale bars, 10 µm. (I)

Legend continued on next page

Figure 2 legend (continued)

Schematic representation showing hypothetical pushing forces (pink arrows) emanating from the GC, straining E-E junctions, leading to fracturing. Ctrl, control; Succ., succinate.

Additionally, GC hypertrophy resulted in an increase in complete (vertex-to-vertex) GAFs (Fig. S3G), consistent with the model's prediction of complete junctional fracture once the GC pressure threshold is exceeded. Fractures also appeared to extend deeper, as indicated by the increased number of fractures at the level of the AJs and the appearance of fractures at the desmosomes (Fig. S5). Importantly, this larger and deeper fracturing was accompanied by a significant increase in intestinal permeability *in vivo* (Fig. 2F), suggesting that GC hypertrophy severely weakens epithelial barrier integrity. At the same time, there was no increase in inflammatory markers or weight loss (Fig. S6 A, B), indicating that the increased fracturing and permeability likely arise from epithelial mechanics rather than disease. To test whether GC hypertrophy compromises tissue integrity under extrinsic mechanical stress, we applied defined flow through the intestinal lumen *ex vivo* using a peristaltic pump system (shear stress estimated at 1Pa) (Fig. 2G). This shear stress challenge resulted in a striking increase in fractures emanating from GCs in tissues from succinate-treated mice, with fractures extending further (≥3 neighboring cells) compared to control tissue, which remained unaffected (Fig. 2H, S6C). Taken together, these data suggest that GCs exert pressure on neighboring enterocytes, leading to junctional ruptures (Fig. 2I), which can be further exacerbated by increased GC volume (goblet hypertrophy). Importantly, we find that this leads to functional consequences, notably an increase in intestinal permeability and heightened susceptibility to mechanical stress from the environment.

Active response of the tissue to goblet cell pressure

Cellular junctions are mechanoresponsive. This response involves different junctional components at different levels (*6*, *24*). E-cadherin, a key marker of AJs, is known to respond to mechanical stress by clustering (*11*). Interestingly, we found a striking increase in E-cadherin junctional levels in GC-adjacent E-E AJs compared to non-adjacent AJs (Fig. 3A, B). Moreover, E-cadherin signal levels were heterogeneous along the junctions, progressively increasing towards the goblet cell (Fig. 3C), a pattern also observed in 2D organoids (Fig. S7). This accumulation prompted us to investigate whether it indicated higher strain near GCs. To test this, we analyzed the distribution of tricellulin, a TCJ marker associated with tension hotspots and mechanical failure points (*25*, *26*). Notably, tricellulin levels were elevated at G-E-E TCJs compared to E-E-E TCJs (Fig. 3D, E). Moreover, the tricellulin signal at the GAFs was disorganized, exhibiting multiple puncta, in contrast to the single puncta observed at unfractured TCJs (Fig. 3D, F), supporting the hypothesis that fractures initiate at the G-E-E TCJ and propagate towards the E-E bicellular junction (Fig. S1C). At the level of desmosomes, we found an 2.8-fold increase in desmocollin – a desmosomal cadherin (*27*) – in GC-adjacent E-E desmosomes (Fig. 3G, H), suggesting local mechanoadaptation of desmosomes. Altogether, our results show that junctional protein accumulation at TCJs, AJs and desmosomes in enterocytes correlates with their proximity to GCs.

We hypothesize that the tissue actively responds by mechanoadaptation to mitigate the stresses arising from goblet cell compression and fracturing.

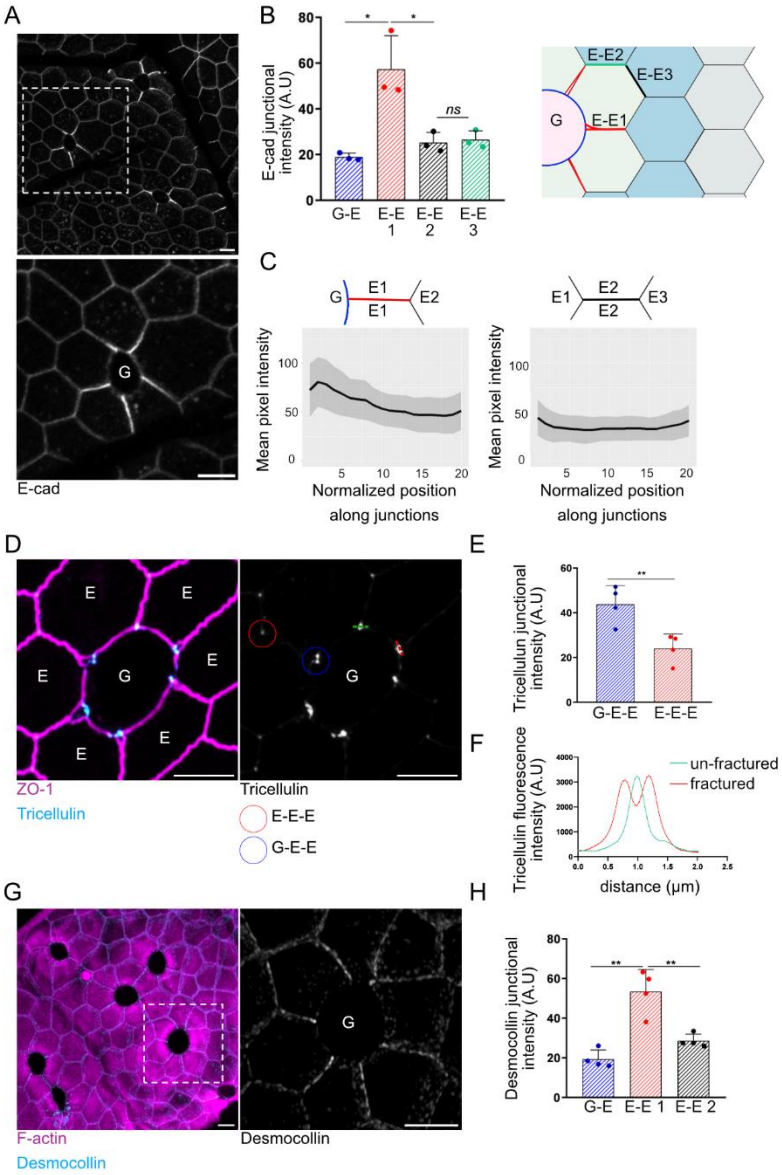

Figure 3: Active mechanoadaptation of the tissue to goblet cell pressure. (A) Representative *en face* image; boxed region is shown in higher magnification. Maximum intensity projection (Z range, 1.8 µm). Scale bars, 5 µm. (B) Bar chart showing average junctional E-cadherin intensity. Multiple t-test. Ns: non-significant, *: $p < 0.05$.; n=3 experiments. (C) Average line intensity profiles for junctional E-cadherin E-E 1st neighbor (left) and E-E 2nd neighbor (right) along rescaled E-E junctions, as indicated. (D) Representative *en face* image; G-E-E are encircled in blue and E-E-E in red. Maximum intensity projection (Z range, 1.4 µm). Scale bars, 5 µm. (E) Bar charts showing average tricellulin intensity in G-E-E or E-E-E TCJs. Unpaired t-test. *: $p < 0.05$; n=4 experiments. (F) Line intensity profiles for tricellulin at fractured (red) and un-fractured (green) tri-cellular junctions; these profiles correspond to lines shown in E. (G) Representative *en face* image; maximum intensity projection (Z range, 1.5 µm). Boxed region is shown in higher magnification. Scale bars, 5 µm. (H) Bar chart displaying average desmocollin junctional intensity. Multiple t-test. **: $p < 0.01$; n=4 experiments.

Goblet cell-associated fracturing depends on mechanical properties of neighboring cells

Because fracturing often correlates with locally increased active stresses generated by actomyosin contractility (*28*), we next investigated whether and how tissue mechanics contribute to GAFs. Consistent with this, we observed E-cadherin junctional increase in GC-adjacent E-E junctions (Fig. 3A), suggesting local mechanical strain. To determine whether there are differences in contractility between GCs and their neighboring enterocytes, we first assessed the levels of non-muscle myosin IIA (NMIIA) in the apical actomyosin belts using live imaging of gut explants derived from mice expressing GFP-tagged endogenous NMIIA (*29*). We found that GCs exhibited higher NMIIA levels in their apical belts compared to the myosin belts of enterocytes (Fig. 4A, B). However, phospho-myosin light chain (T18/S19) (P-MLC) staining, a marker of active myosin, was not detectable in the apical belts of GCs compared to the junctions of neighboring enterocytes (Fig. 4C, D), suggesting lower contractility. To confirm these results and to assess the tensile forces, we performed laser cuts of the individual G-E or surrounding E-E AJ junctions *ex vivo*, in gut explants (*5*) (Fig. S8). The recoil velocity was 4-fold higher at the E-E junctions than at the G-E junctions, indicating that the GC myosin ring does not confer increased contractility. Beyond its role in contractility, myosin II crosslinking of cortical actin filaments is critical for the mechanical properties of cells and junctions (e.g., stiffness/rigidity), which influence cell shape and junctional strength (*30–32*). We hypothesized that epithelial myosin II could therefore significantly influence the formation of GAFs. We tested this using an inducible, intestinal epithelium-specific knockout mouse model of NMIIA ($NMIIA^{KO}$; Fig. 4E, S9A) (*33*). We found that NMIIA depletion resulted in a reduction in GAF area (control: 0.64 μm^2; $NMIIA^{KO}$: 0.33 μm^2) (Fig. 4E, F), and a decrease in E-cadherin enrichment (Fig. S9B, C), while no change in GC mucus volume was detected (Fig. S9D).

This result contradicted our model of finite junctional adhesion under goblet pressure (Theory Note; Fig. S3C), which predicted that decreased junctional stiffness would promote fracture by making junctions more susceptible to deformation from GC pressure. One possible explanation for this shortcoming of our model is that we only considered the mechanics of a single E-E junction, while vertex models emphasize the importance of overall cell shape in dictating tissue dynamics and mechano-response. The shape index, as proposed in vertex models, serves as a key parameter to assess epithelial tissue fluidity and the transition between more rigid and more fluid states, reflecting changes in cellular packing and mechanical interactions (*34–36*). Interestingly, recent theoretical work incorporating fracture into the vertex model suggests that changes in overall rigidity can reduce tissue susceptibility to local fractures (*37*, *38*). To explore this further, we developed simulations of cells as deformable particles with finite adhesion (Theory Note, Fig. S10A). These simulations retained the key physical components of the vertex model – namely, the existence of a preferred cell shape and area – while allowing for complex junctional deformations and ruptures, which were crucial for modeling GC and GAF shapes. We found that two key parameters governed the presence of GAFs: GC size/pressure, as in the previous analytical model, but also the fluidity of the tissue (Fig. 4G).

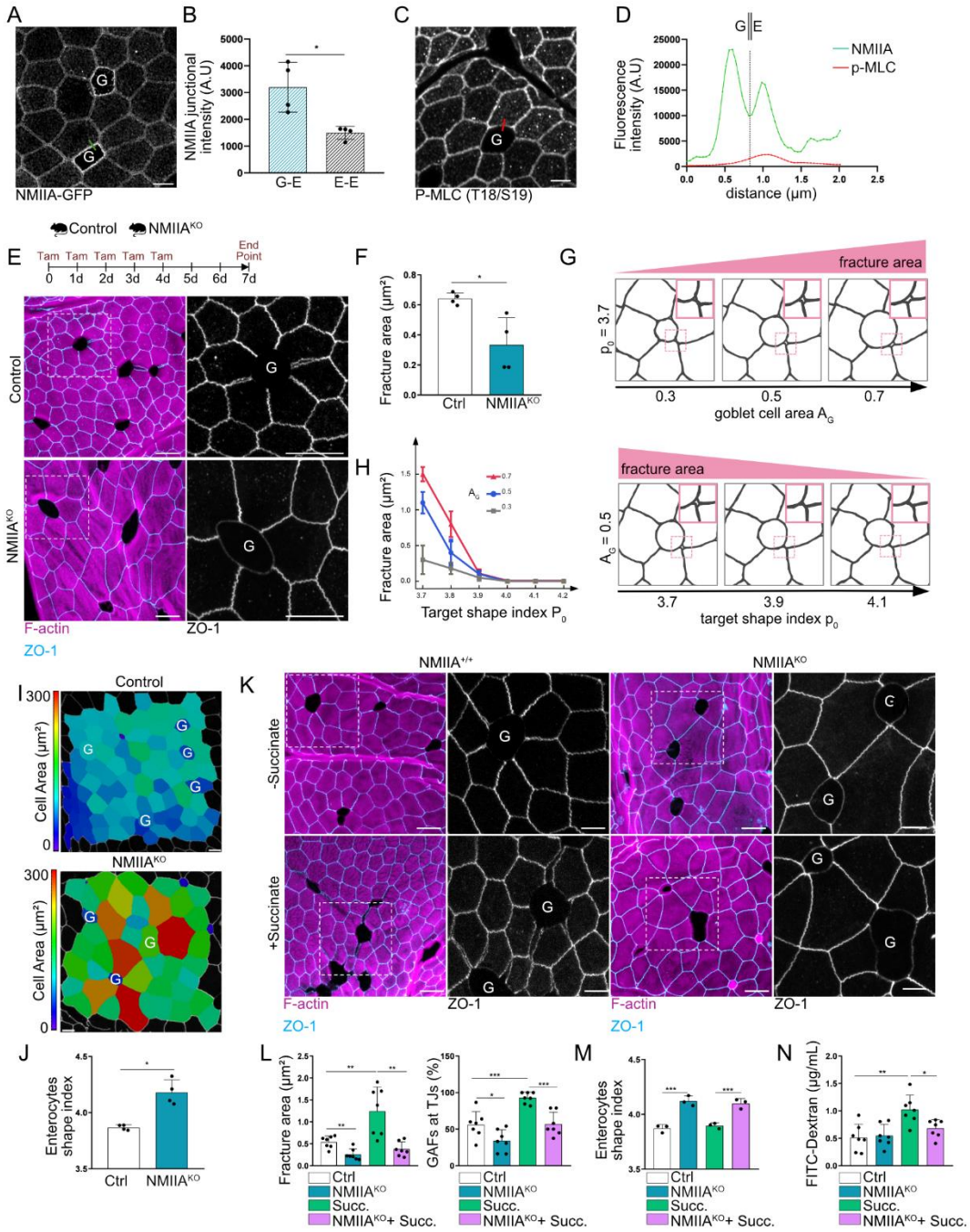

Figure 4: Goblet cell-associated fracturing depends on global tissue mechanical properties. (A) Representative confocal image of live intestinal tissue showing apical NMIIA-GFP signal. Maximum intensity projection (Z range, 1.2 µm). Scale bar, 5 µm. (B) Bar chart displaying average NMIIA junctional intensity. Maximum intensity projection (Z range, 2 µm). Mann-Whitney test, *: $p < 0.05$; n=4 experiments. (C) Representative image showing apical pMLC signal. Scale bar, 5 µm. (D) Line intensity profiles of NMIIA-GFP and phospho-MLC corresponding to lines shown in images A and C. (E) Top: Schematic representation of experimental procedure for NMIIA^{KO} mice, Tam, tamoxifen. Bottom: Representative images from control and NMIIA^{KO} mice. Maximum intensity projection (Z range, 4.5 µm, 3.8 µm). Boxed regions are shown in higher magnification. Scale bars, 10 µm. (F) Bar chart showing average fracture area. Mann-Whitney test. *: $p < 0.05$; n=4 experiments. (G) Simulations of the tissue mechanics model with two main parameters: the goblet cell area A_G and the shape index of enterocytes P_0 (relevant to tissue rheology). The model predicts that GAFs increase with the goblet cell area A_G (cell shape index P_0 =3.7, top panel), but decrease with the

Legend continued on next page

Figure 4 legend (continued)

shape index P_0 (goblet cell area A_G = 0.5, bottom panel). (H) Predicted fracture area as a function of goblet cell area (A_G) and shape index of enterocytes (P_0). (I) Representative heatmap images displaying apical cell area in control and NMIIA^{KO} mice. Scale bars, 5 µm. (J) Bar chart displaying average enterocyte shape index. Mann-Whitney test. *: $p < 0.05$; n=4 experiments. (K) Representative *en face* images from control (NMIIA$^{+/+}$) and NMIIA^{KO} mice, with and without succinate treatment. Scale bars, 10 µm. Boxed regions are shown in higher magnification. Maximum intensity projection (Z range, 3 µm, 3.8 µm, 4.2 µm, 4.5 µm). Scale bars, 5 µm. (L) Bar charts displaying average fracture area (left) and average percentage of GAFs (right), according to the conditions. Multiple t-test, *ns*: non-significant, *: $p<0.05$, **: $p < 0.01$, ***: $p<0.001$, ****<0.0001; n=7 experiments. (M) Bar chart displaying average enterocyte shape index. Multiple t-test. ***: $p < 0.005$; n=3 experiments. (N) Bar chart showing average intestinal permeability. Multiple t-test; *: $p<0.05$, **: $p < 0.01$; n= 7 experiments. Succ., succinate.

Consistent with published simulations of global tissue rupture (*37*), increasing the preferred perimeter of cells above a threshold (increasing fluidity) prevented the formation of GAFs (Fig. 4G, H). This leads to the prediction that NMIIA^{KO} enterocytes should be more fluid, i.e., have a higher shape index. We tested this by segmenting the tissue and found increased apical cell area, but also an increase of cell shape index (control: 3.86; NMIIA^{KO}: 4.18) (Fig. 4I, J; Fig. S9E), confirming our hypothesis from simulations. Together, these results support our hypothesis that, in addition to goblet pressure, fracturing depends on overall cell shape and mechanical properties regulated by myosin II activity.

To further test model predictions and determine whether myosin II depletion could prevent the increased fracturing and barrier breaching observed with GC volume increase (Fig. 2), we induced GC hypertrophy *in vivo* in NMIIA^{KO} mice and in blebbistatin-treated 2D organoids (Fig. S11A, S12A). Hypertrophy-induced GAFs were significantly reduced both *in vivo* and *in vitro* (Fig. 4K, L, S12B-D), including deeper fractures at AJs and desmosomes (Fig. S11B-E). Consistent with our previous findings, NMIIA^{KO} enterocytes, treated or not with succinate, displayed an increased cell shape index compared to control or succinate-treated epithelium (Fig. 4M), further emphasizing the importance of enterocyte rheology in the fracturing process. Importantly, the GC hypertrophy-associated increase in intestinal permeability observed *in vivo* was significantly reduced in NMIIA^{KO} mice (Fig. 4N). Overall, our results indicate that GAF formation depends on both goblet cells and their immediate neighbors – a two-component system in which the goblet cell body pushes and deforms neighboring enterocytes, straining and fracturing their junctions, which depends on tissue rheology controlled by myosin II.

Discussion

Here we show that under homeostatic conditions *in vivo*, intestinal goblet cells (GCs) exert local mechanical compression on adjacent enterocytes due to their bulky shape and volumetric expansion, resulting in fracture of their junctions as a function of enterocyte mechanics controlled by myosin II.

The integrity of the intestinal epithelial barrier is critical for maintaining homeostasis, and its disruption can trigger pathologies such as inflammatory diseases (IBD) and tumorigenesis (*39*). The barrier function of the intestinal epithelium is maintained by adhesive junctional complexes, particularly TJs, which are the primary physical determinant of the epithelial barrier (*8*), assumed to form a continuous, uninterrupted seal between adjacent cells, blocking the passage of bacterial

toxins and pathogens into the underlying tissues (*39*). However, most studies of epithelial cell junctions have focused predominantly on cell lines or single “main” cell types, such as enterocytes, using thin histology sections. In contrast, employing thick tissue sections and 3D confocal microscopy, we found that approximately 50% of GCs are associated with fractures. This also raised a question about the frequency of GC-associated junctional breaching. Examining E-cadherin accessibility in GC-adjacent enterocytes, revealed a significantly higher proportion (80%) with breached TJs. This suggests that GC-associated junctional breaching is much more prevalent than expected based on the detection of GAFs by confocal imaging, possibly due to technical limitations of confocal imaging. Junctional fracturing in epithelial tissues has previously been observed in cultured monolayers subjected to extrinsic stretch (*15*), in placozoans under high motile stress (*38*), and during hydraulic fracturing of blastocysts (*40*). However, goblet cell-associated fractures represent the first example of an adult epithelium undergoing self-induced rupture under homeostatic conditions.

While the epithelial integrity and mechano-responsiveness of individual junction types have been relatively well studied, their comparative adhesive strength and resistance to mechanical stress *in vivo* remain unclear. Interestingly, we found that TJs fracture more frequently (50%) than AJs (18%), while no fractures were observed at the desmosome level under homeostatic conditions. This suggests that TJs are more fragile and less resistant to mechanical stress than the underlying junctions. Notably, fractures predominantly originate at tricellular junctions (TCJs) at the G-E-E interface, before propagating along the E-E bicellular junction. These results are consistent with observations that TCJs are points of high tension in the tissue and may represent "weak spots" in the epithelium that are more prone to fracturing (*25*). Remarkably, we found that enterocytes accumulate the transmembrane proteins E-cadherin and desmocollin in response to the presence of GCs, suggesting junctional reinforcement, as previously demonstrated *in vitro* (*11*). This accumulation of junctional proteins may serve to increase junctional strength and prevent further rupture.

Junctional reinforcement has previously been described as a response to increased tension (*14*), suggesting that GC contractility may play a role. However, the prominent apical myosin ring in GCs does not appear to be contractile, leading us to speculate that it has a more passive, scaffolding role in containing mucus granules within the cell. In addition, we found that GAFs depend on global tissue mechanical properties (i.e., solidity/fluidity), which we manipulated by perturbing myosin II. Reduced myosin expression or activity *in vivo* resulted in a more fluid tissue that was less prone to rupture. This finding is in line with recent *in vitro* experimental work (*15*) and theoretical studies of rupture in epithelia (*37*), which show that myosin and the associated solid- or fluid-like state of the tissue play a critical role in fracturing processes.

The presence of GCs is necessary for fractures to occur, as no fractures were detected in their absence. Our results indicate that fractures are promoted by the volume of GCs and the pressure they exert on neighboring enterocytes. In our study, succinate treatment was used to mimic parasitic infection, a condition previously described as inducing GC hyperplasia and

hypertrophy, leading to an increase in GC numbers and mucus hypersecretion, respectively, which promotes parasite clearance through the "weep and sweep" response (*22*, *41*). Unexpectedly, however, we did not observe GC hyperplasia in our experiments. This discrepancy may be due to our use of whole-mount staining (thick sections) rather than the thin histology sections to assess GC numbers. Nevertheless, we observed prominent GC hypertrophy, characterized by an increase in intracellular mucus volume. Paradoxically, GC hypertrophy was closely associated with a significant increase in fracture size (both area and depth) and number, ultimately leading to increased intestinal permeability. This challenges the widely held view that GC hypertrophy is solely protective. Despite the increased permeability in succinate treatments, no signs of inflammation were observed. We speculate that pathogen-induced GC hypertrophy would lead to increased translocation of microbes and toxins, resulting in inflammation. Also, we speculate that mucus hypersecretion may compensate for GC hypertrophy-induced fracturing by enhancing microbial trapping. Notably, when luminal shear stress was applied *ex vivo*, GC hypertrophy severely compromised tissue integrity, creating large intercellular gaps that spanned multiple rows of adjacent cells. Elevated shear stress could occur in partial intestinal obstructions and luminal narrowing due to inflammation, fibrosis, strictures and tumors, whereby fluid velocity increases. These findings suggest that an increase in GC volume (hypertrophy) is necessary and sufficient to increase fracturing and weaken the intestinal epithelium, making it more vulnerable to mechanical insults, which could further exacerbate damage and trigger inflammation.

GCs have been identified as entry points for *Listeria monocytogenes* invasion and infection (*21*), a process that requires accessible E-cadherin. This is consistent with our findings of GAFs and the associated barrier breach, which could expose E-cadherin and facilitate bacterial adhesion and tissue infection. GCs have also been identified as mediators of interactions between the immune system and luminal content through the formation of goblet cell-associated antigen passages (GAPs), which enable the sampling of luminal antigens and their delivery to underlying immune cells via transcytosis (*42*). The junctional fractures (GAFs) described here may have a similar function, physically facilitating antigen sampling by immune cells. However, we have also observed GAFs in the embryonic mouse intestine, where the lumen is empty, and neither the immune system nor the microbiota are present. Therefore, we propose that GAFs primarily act as a mechanical buffer, absorbing pressure and alleviating mechanical challenges at the G-E interface. Remarkably, GAFs were observed in both mouse and human intestinal tissue, suggesting it may be conserved across species.

Our results demonstrate that goblet cells unexpectedly challenge the intestinal epithelial barrier by creating structural vulnerabilities that may contribute to intestinal pathologies, including infection, inflammation and disease progression. In conclusion, we show that the mechanical interplay between goblet cells and neighboring enterocytes promotes junctional fractures, compromising the epithelial barrier. We propose that the mechanical properties of individual cells — both goblet cells and enterocytes — are key factors in maintaining junctional integrity and preserving the intestinal epithelial barrier.

Acknowledgments
We thank E. Hannezo, M. Suzanne, B. Bénazéraf, E. Theveneau, A. Davy, R. Galupa, and all members of the Krndija lab for their critical feedback and valuable suggestions. We acknowledge the help and contribution of the ANEXPLO mouse facility, Light Imaging Toulouse CBI (LITC) facility at the CBI, and TRI-IPBS imaging facility (supported by the French National Research Agency — ANR-24-INBS-00005 FBI Biogen), members of the national infrastructure France-BioImaging. Special thanks to Laurent Malaquin (LAAS) for luminal shear stress simulations, Alexandre Lucas (We-Met platform, I2MC, Toulouse) for conducting the ELISA tests, and Silvia Kočanová for assistance in acquiring human samples.

Funding: This work was supported by the CNRS ATIP-Avenir grant (D.K.), ANR (ANR-23-CE13-0005 GOBLET) grant (D.K.) and FRM fellowship (V.K.).

Author contributions: Conceptualization: D.K.; Methodology: J.C., Y.H., S.-L.X., D.K.; Investigation: J.C., S.N., S.B.F., V.K., T.M., S.-L.X., E.B.; Project administration: J.C., D.K.; Supervision: S.-L.X., D.K.; Funding acquisition: D.K.; Writing – original draft: J.C., D.K.; Writing – review & editing: J.C., D.K.

Competing interests: The authors declare no competing interests.

Data and materials availability: All data are available in the main text or the supplementary materials.

References

1. A. M. Marchiando, W. V. Graham, J. R. Turner, Epithelial barriers in homeostasis and disease. *Annu Rev Pathol* **5**, 119–144 (2010).
2. J. R. Turner, Intestinal mucosal barrier function in health and disease. *Nat Rev Immunol* **9**, 799–809 (2009).
3. C. P. Gayer, M. D. Basson, The effects of mechanical forces on intestinal physiology and pathology. *Cellular Signalling* **21**, 1237–1244 (2009).
4. R. M. Houtekamer, M. C. van der Net, M. M. Maurice, M. Gloerich, Mechanical forces directing intestinal form and function. *Current Biology* **32**, R791–R805 (2022).
5. D. Krndija, F. El Marjou, B. Guirao, S. Richon, O. Leroy, Y. Bellaiche, E. Hannezo, D. Matic Vignjevic, Active cell migration is critical for steady-state epithelial turnover in the gut. *Science* **365**, 705–710 (2019).
6. B. Ladoux, R.-M. Mège, Mechanobiology of collective cell behaviours. *Nat Rev Mol Cell Biol* **18**, 743–757 (2017).
7. D. Pinheiro, Y. Bellaïche, Mechanical Force-Driven Adherens Junction Remodeling and Epithelial Dynamics. *Developmental Cell* **47**, 391 (2018).
8. S. Citi, M. Fromm, M. Furuse, L. González-Mariscal, A. Nusrat, S. Tsukita, J. R. Turner, A short guide to the tight junction. *Journal of Cell Science* **137**, jcs261776 (2024).
9. C. Guillot, T. Lecuit, Mechanics of epithelial tissue homeostasis and morphogenesis. *Science* **340**, 1185–1189 (2013).

10. B. D. Hoffman, A. S. Yap, Towards a Dynamic Understanding of Cadherin-Based Mechanobiology. *Trends in Cell Biology* **25**, 803–814 (2015).
11. T. Lecuit, A. S. Yap, E-cadherin junctions as active mechanical integrators in tissue dynamics. *Nat Cell Biol* **17**, 533–539 (2015).
12. N. Borghi, M. Sorokina, O. G. Shcherbakova, W. I. Weis, B. L. Pruitt, W. J. Nelson, A. R. Dunn, E-cadherin is under constitutive actomyosin-generated tension that is increased at cell–cell contacts upon externally applied stretch. *Proceedings of the National Academy of Sciences* **109**, 12568–12573 (2012).
13. S. Citi, The mechanobiology of tight junctions. *Biophys Rev* **11**, 783–793 (2019).
14. G. Charras, A. S. Yap, Tensile Forces and Mechanotransduction at Cell–Cell Junctions. *Current Biology* **28**, R445–R457 (2018).
15. J. Duque, A. Bonfanti, J. Fouchard, L. Baldauf, S. R. Azenha, E. Ferber, A. Harris, E. H. Barriga, A. J. Kabla, G. Charras, Rupture strength of living cell monolayers. *Nat. Mater.* **23**, 1563–1574 (2024).
16. B. N. Nanavati, I. Noordstra, A. K. O. Lwin, J. W. Brooks, J. Rae, R. G. Parton, S. Verma, K. Duszyc, K. J. Green, A. S. Yap, The desmosome-intermediate filament system facilitates mechanotransduction at adherens junctions for epithelial homeostasis. *Current Biology* **34**, 4081-4090.e5 (2024).
17. R. D. Specian, M. G. Oliver, Functional biology of intestinal goblet cells. *Am J Physiol* **260**, C183-193 (1991).
18. J. K. Gustafsson, M. E. V. Johansson, The role of goblet cells and mucus in intestinal homeostasis. *Nat Rev Gastroenterol Hepatol* **19**, 785–803 (2022).
19. H. Gehart, H. Clevers, Tales from the crypt: new insights into intestinal stem cells. *Nat Rev Gastroenterol Hepatol* **16**, 19–34 (2019).
20. C. Pérez-González, G. Ceada, F. Greco, M. Matejčić, M. Gómez-González, N. Castro, A. Menendez, S. Kale, D. Krndija, A. G. Clark, V. R. Gannavarapu, A. Álvarez-Varela, P. Roca-Cusachs, E. Batlle, D. M. Vignjevic, M. Arroyo, X. Trepat, Mechanical compartmentalization of the intestinal organoid enables crypt folding and collective cell migration. *Nat Cell Biol* **23**, 745–757 (2021).
21. G. Nikitas, C. Deschamps, O. Disson, T. Niault, P. Cossart, M. Lecuit, Transcytosis of Listeria monocytogenes across the intestinal barrier upon specific targeting of goblet cell accessible E-cadherin. *J Exp Med* **208**, 2263–2277 (2011).
22. W. Lei, W. Ren, M. Ohmoto, J. F. Urban, I. Matsumoto, R. F. Margolskee, P. Jiang, Activation of intestinal tuft cell-expressed Sucnr1 triggers type 2 immunity in the mouse small intestine. *Proc Natl Acad Sci U S A* **115**, 5552–5557 (2018).
23. X. Yin, H. F. Farin, J. H. van Es, H. Clevers, R. Langer, J. M. Karp, Niche-independent high-purity cultures of Lgr5+ intestinal stem cells and their progeny. *Nat Methods* **11**, 106–112 (2014).
24. N. Osmani, M. Labouesse, Remodeling of keratin-coupled cell adhesion complexes. *Current Opinion in Cell Biology* **32**, 30–38 (2015).
25. F. Bosveld, Y. Bellaïche, Tricellular junctions. *Current Biology* **30**, R249–R251 (2020).
26. L. van den Goor, J. Iseler, K. M. Koning, A. L. Miller, Mechanosensitive recruitment of Vinculin maintains junction integrity and barrier function at epithelial tricellular junctions. *Current Biology* **34**, 4677-4691.e5 (2024).
27. A. L. Perl, J. L. Pokorny, K. J. Green, Desmosomes at a glance. *Journal of Cell Science* **137**, jcs261899 (2024).

28. A. Bonfanti, J. Duque, A. Kabla, G. Charras, Fracture in living tissues. *Trends in Cell Biology* **32**, 537–551 (2022).
29. Y. Zhang, M. A. Conti, D. Malide, F. Dong, A. Wang, Y. A. Shmist, C. Liu, P. Zerfas, M. P. Daniels, C.-C. Chan, E. Kozin, B. Kachar, M. J. Kelley, J. B. Kopp, R. S. Adelstein, Mouse models of MYH9-related disease: mutations in nonmuscle myosin II-A. *Blood* **119**, 238–250 (2012).
30. P. Chugh, E. K. Paluch, The actin cortex at a glance. *Journal of Cell Science* **131**, jcs186254 (2018).
31. J.-L. Maître, H. Berthoumieux, S. F. G. Krens, G. Salbreux, F. Jülicher, E. Paluch, C.-P. Heisenberg, Adhesion Functions in Cell Sorting by Mechanically Coupling the Cortices of Adhering Cells. *Science* **338**, 253–256 (2012).
32. G. Salbreux, G. Charras, E. Paluch, Actin cortex mechanics and cellular morphogenesis. *Trends Cell Biol* **22**, 536–545 (2012).
33. J. Jacobelli, R. S. Friedman, M. A. Conti, A.-M. Lennon-Dumenil, M. Piel, C. M. Sorensen, R. S. Adelstein, M. F. Krummel, Confinement-Optimized 3-Dimensional T cell Amoeboid Motility is Modulated via Myosin IIA-Regulated Adhesions. *Nat Immunol* **11**, 953–961 (2010).
34. J.-A. Park, J. H. Kim, D. Bi, J. A. Mitchel, N. T. Qazvini, K. Tantisira, C. Y. Park, M. McGill, S.-H. Kim, B. Gweon, J. Notbohm, R. Steward Jr, S. Burger, S. H. Randell, A. T. Kho, D. T. Tambe, C. Hardin, S. A. Shore, E. Israel, D. A. Weitz, D. J. Tschumperlin, E. P. Henske, S. T. Weiss, M. L. Manning, J. P. Butler, J. M. Drazen, J. J. Fredberg, Unjamming and cell shape in the asthmatic airway epithelium. *Nature Mater* **14**, 1040–1048 (2015).
35. D. Bi, X. Yang, M. C. Marchetti, M. L. Manning, Motility-driven glass and jamming transitions in biological tissues. *Phys Rev X* **6**, 021011 (2016).
36. E. Hannezo, C.-P. Heisenberg, Rigidity transitions in development and disease. *Trends Cell Biol* **32**, 433–444 (2022).
37. Y. Chen, Q. Gao, J. Li, F. Mao, R. Tang, H. Jiang, Activation of Topological Defects Induces a Brittle-to-Ductile Transition in Epithelial Monolayers. *Phys. Rev. Lett.* **128**, 018101 (2022).
38. V. N. Prakash, M. S. Bull, M. Prakash, Motility-induced fracture reveals a ductile-to-brittle crossover in a simple animal's epithelia. *Nat. Phys.* **17**, 504–511 (2021).
39. M. A. Odenwald, J. R. Turner, The intestinal epithelial barrier: a therapeutic target? *Nat Rev Gastroenterol Hepatol* **14**, 9–21 (2017).
40. J. G. Dumortier, M. Le Verge-Serandour, A. F. Tortorelli, A. Mielke, L. de Plater, H. Turlier, J.-L. Maître, Hydraulic fracturing and active coarsening position the lumen of the mouse blastocyst. *Science* **365**, 465–468 (2019).
41. C. Sharpe, D. J. Thornton, R. K. Grencis, A sticky end for gastrointestinal helminths; the role of the mucus barrier. *Parasite Immunol* **40**, e12517 (2018).
42. J. R. McDole, L. W. Wheeler, K. G. McDonald, B. Wang, V. Konjufca, K. A. Knoop, R. D. Newberry, M. J. Miller, Goblet cells deliver luminal antigen to CD103+ dendritic cells in the small intestine. *Nature* **483**, 345–349 (2012).